

# Development of a Method for the Observation of Lightning in Protoplanetary Disks Using Ion Lines

Takayuki Muranushi

RIKEN Advanced Institute for Computational Science, 7-1-26, Minatojima-minami-machi,  
Chuo-ku, Kobe, Hyogo, 650-0047, Japan; takayuki.muranushi@riken.jp

Eiji Akiyama

National Astronomical Observatory of Japan, 2-21-1 Osawa, Mitaka, Tokyo 181-8588,  
Japan; eiji.akiyama@nao.ac.jp

Shu-ichiro Inutsuka

Nagoya University, Furo-cho, Chikusa-ku, Nagoya, 464-8601, Japan;  
inutsuka@nagoya-u.ac.jp

Hideko Nomura

Department of Earth and Planetary Sciences, Tokyo Institute of Technology,  
nomura@geo.titech.ac.jp

and

Satoshi Okuzumi

Department of Earth and Planetary Sciences, Tokyo Institute of Technology,  
okuzumi@geo.titech.ac.jp

Received \_\_\_\_\_; accepted \_\_\_\_\_

## ABSTRACT

In this paper, we propose observational methods for detecting lightning in protoplanetary disks. We do so by calculating the critical electric field strength in the lightning matrix gas (LMG), the parts of the disk where the electric field is strong enough to cause lightning. That electric field accelerates multiple positive ion species to characteristic terminal velocities. In this paper, we present three distinct discharge models, with corresponding critical electric fields. We simulate the position-velocity diagrams and the integrated emission maps for the models. We calculate the measure of sensitivity values for detection of the models, and for distinguishing between the models. At the distance of TW-Hya (54pc), LMG that occupies  $2\pi$  in azimuth and  $25\text{au} < r < 50\text{au}$  is  $1200\sigma$ - to  $4000\sigma$ -detectable. The **lower** limits of the radii of  $5\sigma$ -detectable LMG clumps are between 1.6 au and 5.3 au, depending on the models.

*Subject headings:* Dust — planets and satellites:formation — planetary systems: protoplanetary disks — MHD — instabilities

## 1. INTRODUCTION

Lightning in protoplanetary disks is one of the important topic in protoplanetary disk physics. The existence of lightning is still an open question, and if it exists, it serves as one of the elementary electromagnetic processes, as one of the observational clue to measure the electromagnetic states of the disk, and as one of the candidate mechanism for chondrule heating. The observation data available today is huge, and open access to the observational results from the most advanced telescopes are available. However, observation methods of the protoplanetary lightning using the advanced telescopes have not been seriously studied.

There has been a controversial debate on the existence and the mechanism of protoplanetary disk lightning. Gibbard et al. (1997) argued that plasma conductivity is too large for the lightning to take place. Pilipp et al. (1998) argued that unknown, efficient grain-grain charging process is required to produce lightning. Despite of these barriers, mechanisms that lead to lightning are proposed: dust-dust collisional charging (Desch & Cuzzi 2000; Muranushi 2010); mutual positive feedback of thermal ionization and Joule heating (Hubbard et al. 2012; McNally et al. 2013); electric field generated by magnetorotational instability (MRI) (Inutsuka & Sano 2005; Muranushi et al. 2012). Magnetized chondrules included in meteorites carry evidences of 500-1000G magnetic field during chondrule formation, suggesting that they are struck by lightning (Wasilewski & Dickinson 2000).

Meanwhile, the understanding of the lightning ignition mechanism have progressed in these twenty years. Attempts have been made to explain the mechanism that causes discharge at the point well below the nominal dielectric strength of air (Phelps 1971; Nasser 1968). As result, new lightning models such as Runaway breakdown (Gurevich et al. 1992; Gurevich & Zybin 2001) have been proposed. We adopt such progresses in understanding terrestrial lightning, and propose a new observation method for the observational

discrimination of the protoplanetary disk lightning. Observational studies searching for the disk lightning will contribute to the understanding of the electromagnetic process in the protoplanetary disk, and the source of chondrule heating.

Lightning, or electrical breakdown is a result of large electric field  $E$ . Electric field  $E$  in protoplanetary disk can be generated by magnetorotational instability (MRI) or by the collective motion of charged dust. The breakdown model sets an upper limit  $E \leq E_{\text{crit}}$  to the electric field amplitude. At the point  $E = E_{\text{crit}}$  electric discharge takes place, which increases the ionization degree of the medium and prevents the further growth of the electric field amplitude. Thus, electric field amplitude is kept under the upper limit ( $E \leq E_{\text{crit}}$ ) .

This electric field is a common feature of the large volume of gas surrounding the lightning bolts. In this study, we study this electric-field feature as the possible predominant observational signals emitters.

Lightning bolt themselves are difficult to observe because lightning is transient events, and typical radius of a lightning bolt is  $5 \times 10^3$  times mean free path (Pilipp et al. 1992). This radius is much smaller than the scale height of the disk. Hence even if the critical condition is met, most of the time most of the protoplanetary disk gas is in the region outside the lightning bolts. We call this lightning matrix gas (LMG). Properties of LMG is no different from those of the disk gas without lightning, but differ in one point that LMG is subject to critical electric field  $E \lesssim E_{\text{crit}}$ . In this paper, we explore the possible observational features of the LMG.

This paper is organized as follows. In section 2, we introduce the discharge models, taking the Earth atmosphere as an example (§2.1, 2.2); introduce the protoplanetary disk model (§2.3); apply the discharge model to the disk gas (§2.4). In section 3 we establish our observation model by

1. calculating the terminal velocity of the ion molecules §3.1 ,
2. estimating the spectral irradiance §3.2 ,
3. constructing integral maps by radiative transfer simulations §3.3.

Given the simulated observational signals, we estimate the measure-of-sensitivity by matched filtering (§3.4). Finally, in section 3, we conclude and discuss the future directions of this research.

## 2. MODEL

### 2.1. Dielectric Strength of Air

We begin by estimating the dielectric strength of the Earth atmosphere, in order to introduce the reader to the discharge models we later apply to the protoplanetary disk gas.

Dielectric strength of an insulating material is the maximum amplitude of the electric field that does not cause electric breakdown in the material. It is a physical property of central importance for the discharge physics. Lightning on Earth is a discharge phenomenon in the air. However, it has been a long standing mystery that lightning takes place under electric field amplitude well below the dielectric strength of the air measured in the laboratory.

The dielectric strength of the air at Normal Temperature and Pressure (NTP; 20°C and 1atm) are well established from laboratory experiments (Rigden 1996):

$$E_0 = 30\text{kV/cm.} \tag{1}$$

The long-distance limit of Paschen’s law states that the dielectric strength of gas depends linearly on the gas number density (Raizer 1997). However, in the case of the Earth

atmosphere the dependence of the dielectric strength on the number density is known to be steeper than linear. This is explained by the effects of electron loss via three-body interactions and also collisions to the water vapor molecules. Empirical formulae are known (Phelps & Griffiths 1976; Takahashi 2009):

$$E = E_0 \left( \frac{P}{P_0} \right)^{1.5-1.65}, \quad (2)$$

where  $E_0$  and  $P_0$  are the dielectric strength and the pressure of the air at ground level, respectively. The formula predicts the dielectric strength of the air to be 17kV/cm and 10kV/cm at altitudes 3km and 6km, respectively.

On the other hand, intracloud lightning is observed with electric field amplitude of 140V/cm (French et al. 1996) to 150V/cm (Dye et al. 1986). Cloud-to-ground lightning is observed with electric field amplitude of around 1kV/cm (Takahashi 1983) to 2kV/cm (Takahashi et al. 1999) .

## 2.2. Breakdown Models on Earth

In this section we introduce three breakdown models we are going to compare in this paper. Note that in our formulation, the density functions of electrons and ions under given electric field are well-understood (see e.g. Golant et al. (1980)), and thus we use the same density function for all the three breakdown models. What we do not understand well is the dielectric strength — the amplitude of the electric field at which breakdown takes place. The only difference among the three models is the assumed value of the dielectric strength.

[T] In *Townsend breakdown model* the critical electric field is such that an electron accelerated by the electric field over its mean free path gains kinetic energy large enough to ionize a neutral gas molecule. It has widely been used in the meteorological context, and also adopted into astrophysical context e.g. by Desch & Cuzzi (2000);

Muranushi (2010) . This model explains laboratory gas discharge experiments (equation (1)) well.

- [DP] Druyvesteyn & Penning (1940) has derived the formulae for equilibrium distribution of electrons under constant electric field, neglecting the effects of inelastic collision with atoms. When the electric field is weak, so that the work done by the electric field per mean free path  $eEl_{\text{mfp}}$  is much smaller than the electron kinetic energy, the equilibrium distribution is nearly isotropic. The distribution is expressed as the sum of the isotropic equilibrium and its first-order perturbation. The average energy and the average velocity of the mean motion,  $\langle \epsilon \rangle$  and  $\langle v_z \rangle$ , satisfy  $\langle \epsilon \rangle = 0.43eEl_{\text{mfp}}\sqrt{M/m_e}$  and  $\langle v_z \rangle = 0.9\sqrt{eEl_{\text{mfp}}}(m_eM)^{-1/4}$ , respectively. Here,  $m_e$  and  $M$  are the masses of the electron and the collision partner, respectively.

*Druyvesteyn-Penning (DP) breakdown model* assumes that the breakdown takes place when  $\langle \epsilon \rangle$  exceeds the ionization energy. Since the factor  $\sqrt{M/m_e}$  makes the average energy  $\langle \epsilon \rangle$  in DP breakdown model nearly 100 times larger than that in Townsend breakdown model, DP breakdown model allows for breakdown under electric field amplitude at about  $10^{-2}$  times that of the Townsend breakdown model. The model is introduced as a protoplanetary disk lightning model by Inutsuka & Sano (2005).

- [R] Gurevich et al. (1992) have proposed the *runaway breakdown model* and Gurevich & Zybin (2001) provided a detailed review of the model. In this model, the equilibrium of the electrons with relativistic ( $\sim 1\text{MeV}$ ) kinetic energy, much larger than the average of Maxwellian energy distribution, plays an important role. Because the ionization losses for electrons is inversely proportional to the kinetic energy in the non-relativistic regime, the mean free path for such fast electrons is much longer than that for thermal electrons. In the runaway breakdown model, the exponential growth of the number of relativistic electrons takes place, once the

electric field is large enough to balance the ionization losses for certain energy range of the relativistic electrons. (We define that the acceleration criteria is met for those electrons.) The ionization processes generate spectrum of fast and slow electrons. Fast electrons that meets the acceleration criteria contribute to the exponential growth, while the slow electrons are large in number, and increase the ionization degree of the matter and ultimately lead to the electric breakdown of the matter. Thus, runaway breakdown can take place at an electric field value much weaker than that of a Townsend breakdown. The runaway breakdown model better explains the lightning observations in the Earth’s atmosphere and is used as the discharge model in thunderstorm simulations studies, e.g. by Mansell et al. (2002).

In order to estimate the dielectric strength of gas, we need to compute the energy distribution of electrons. Since the interactions of electrons with even the simplest atoms and molecules have profound details (Itikawa. 2000, 2001; Martienssen 2003), this requires difficult numerical computations (Chantry 1981). In this paper, we will instead resort to a simple calculation that reproduces the observed values from the discharge models.

First, we derive the dielectric strength of air at ground level from the Townsend model. Air consists of 78% N<sub>2</sub>, 21% O<sub>2</sub>, and 1% Ar (volume fractions). Air number density at NTP is  $2.504 \times 10^{19} \text{cm}^{-3}$ . The ionization energy of these chemical species are  $\Delta W_{\text{N}_2} = 15.6 \text{ eV}$ ,  $\Delta W_{\text{O}_2} = 12.1 \text{ eV}$ , and  $\Delta W_{\text{Ar}} = 15.8 \text{ eV}$ , respectively. Of these  $\Delta W_{\text{O}_2} \sim 12 \text{ eV}$  is the smallest, so we estimate the electric field amplitude  $E_{\text{crit}}$  required to accelerate the electron up to 12eV; i.e. we solve  $12 \text{ eV} = eE_{\text{crit}}l_{\text{mfp}}$ . The inelastic collisional cross sections ( $\sigma_{\text{inel}}$ ) of N<sub>2</sub>, O<sub>2</sub>, Ar for 12 eV electrons are 0.8, 1.8,  $0.0 \times 10^{-16} \text{cm}^{-2}$  (Itikawa. 2000; Martienssen 2003). Therefore, the mean inelastic cross section of air for 12eV electrons is  $1.0 \times 10^{-16} \text{cm}^{-2}$ . Therefore,  $l_{\text{mfp}} = (n_n \sigma_{\text{inel}})^{-1} = 4.0 \times 10^{-4} \text{cm}$ . This gives

$$E_{\text{crit}} = 30 \text{ kV/cm}, \tag{3}$$



which is in agreement with the dielectric strength of air at ground level (equation (1)).

On the other hand, according to Druyversteyn-Penning model , average kinetic energy of electron under the electric field  $E$  is (Inutsuka & Sano 2005)

$$\langle \epsilon \rangle = 0.43eEl_{\text{mfp}}\sqrt{\frac{M}{m_e}}, \quad (4)$$

where  $M$  is the mass of the collision partner, and the dielectric strength  $E_{\text{crit}}$  is the solution of  $\langle \epsilon \rangle = \Delta W$ . In the case of the air at NTP, since mean molecular weight of air is 28.96 g/mol,  $M = 4.81 \times 10^{-23}$  g. Note that  $l_{\text{mfp}}$  in Druyversteyn-Penning model means elastic mean free path  $l_{\text{mfp}} = (n_n \sigma_{el})^{-1} = 3.59 \times 10^{-5}$  cm.  $l_{\text{mfp}}$  is calculated from elastic cross sections of the elemental molecules at 12eV ( $\sigma_{el} = 1.16 \times 10^{-15}$  cm<sup>2</sup>,  $9.00 \times 10^{-16}$  cm<sup>2</sup>,  $1.74 \times 10^{-15}$  cm<sup>2</sup>, respectively, for N<sub>2</sub>, O<sub>2</sub>, Ar, see Itikawa. (2000); Martienssen (2003).) Therefore,  $E_{\text{crit}} = 3.38$  kV/cm.

Finally, according to the runaway breakdown model the dielectric strength  $E_{\text{crit}}$  is the electric field amplitude where the acceleration by the electric field balances the ionization loss for minimum ionizing electrons. Minimum ionizing electrons are electrons with such kinetic energy  $\varepsilon$  that for them the ionization loss is the smallest. The kinetic energy of the minimum ionizing electrons is about 1MeV, where ionization loss is the dominant energy sink for the electrons (Gurevich & Zybin 2001) . The ionization loss of an electron per unit time as a function of  $\varepsilon$  is formalized by Bethe (1930, 1932); Bloch (1933). We use the following form of Bethe formula from Longair (2010, chap 5.5):

$$-\frac{d\varepsilon}{dx} = \frac{e^4 \bar{Z} n_n}{8\pi \epsilon_0^2 m_e c^2} a(\gamma), \quad (5)$$

$$\text{where } a(\gamma) = \left(\frac{c}{v}\right)^2 \left[ \ln \frac{\gamma^3 m_e^2 v^4}{2(1+\gamma)\bar{I}^2} - \left(\frac{2}{\gamma} - \frac{1}{\gamma^2}\right) \ln 2 + \frac{1}{\gamma^2} + \frac{1}{8} \left(1 - \frac{1}{\gamma}\right)^2 \right]. \quad (6)$$

Here,  $\gamma = (1 - v^2/c^2)^{-1/2}$  is the Lorentz factor of the electron,  $\varepsilon = (\gamma - 1)m_e c^2$  is the electron kinetic energy,  $\bar{Z} n_n$  is the number density of ambient electrons of the matter.  $\bar{I}$  is

the mean excitation energy, a parameter to be fitted to laboratory experimental data. We use the value of  $\bar{I}_{\text{air}} = 86.3\text{eV}$  from ESTAR database (Berger et al. 2009).

For the case of the air  $a(\gamma)$  takes its minimum  $a_{\text{min}} = 20.2$  at  $\gamma = 3.89$  or  $\varepsilon = 1.48\text{MeV}$ . The dielectric strength  $E_{\text{crit}}$  is the solution of the following work-balance equation

$$eE - \frac{d\varepsilon}{dx} = 0, \quad (7)$$

which is

$$\begin{aligned} E_{\text{crit}} &= \frac{e^3 \bar{Z} n_n}{8\pi\epsilon_0^2 m_e c^2} a_{\text{min}}, \\ &= 1.9 \text{ kV/cm}. \end{aligned} \quad (8)$$

Here we summarize the three models. The dielectric strength of the gas is proportional to the number density of the gas. It is this proportional relation that leads to the constant ion velocity we present in this paper.

$$\begin{aligned} E_{\text{c,T}} &= \frac{\Delta W}{e} \sigma_{\text{inel}} n_n = 30.1 \text{ kV/cm} \cdot \left( \frac{n_n}{n_{0,\text{air}}} \right)^1, \\ E_{\text{c,DP}} &= \frac{\Delta W}{0.43} \sqrt{\frac{m_e}{M}} \sigma_{\text{el}} n_n = 3.4 \text{ kV/cm} \cdot \left( \frac{n_n}{n_{0,\text{air}}} \right)^1, \\ E_{\text{c,R}} &= \frac{e^3 a_{\text{min}} \bar{Z}}{8\pi\epsilon_0 m c^2} n_n = 1.9 \text{ kV/cm} \cdot \left( \frac{n_n}{n_{0,\text{air}}} \right)^1. \end{aligned} \quad (9)$$

### 2.3. The Disk Model

The minimum-mass solar nebula (MMSN) model (Hayashi 1981) has been widely used in studies of the protoplanetary disk, with fruitful results. Recent observations have contributed to sophistication of the disk models, and have also reported qualitative values for the inner and outer edge radius of the disks (Kitamura et al. 2002; Andrews et al. 2009, 2010; Williams & Cieza 2011). However, such observational values for geometry and mass

of specific objects still contain uncertainty factors of 2-3, and are subjects of debate. See e.g. Menu et al. (2014).

Some of the features common to the recent models are that the power-law indices of the surface density distribution is close to 1 rather than 1.5, and that there are exponential cut-off at the outer edge of the disk. Therefore, we use simple model proposed by Akiyama et al. (2013) that captures these common features, and adopt the values of TW Hya reported by Calvet et al. (2002). Our disk model is as follows:

$$\begin{aligned}\Sigma(r) &= 6.4 \times 10^2 \left(\frac{r}{1\text{au}}\right)^{-1} \exp\left(-\frac{3r}{r_{\text{out}}}\right) \text{g/cm}^2 && \text{for } r > r_{\text{in}}, \\ \Sigma(r) &= 0 && \text{otherwise,}\end{aligned}\tag{10}$$

$$T(r) = 273 \left(\frac{r}{1\text{au}}\right)^{-\frac{1}{2}} \text{K}.\tag{11}$$

Here,  $r_{\text{out}} = 150\text{au}$  is the outer radius of our model disk. We also introduce an inner cutoff at  $r_{\text{in}} = 3.5\text{au}$ . The assumption of the hydrostatic equilibrium leads to the vertical distribution of the gas

$$\begin{aligned}\rho(r, z) &= \rho_0(r) \exp\left(-\frac{z^2}{2h^2}\right) \\ &= 5.08 \times 10^{-10} \left(\frac{r}{1\text{au}}\right)^{-\frac{3}{2}} \exp\left(-\frac{z^2}{2h^2}\right) \text{g cm}^{-3},\end{aligned}\tag{12}$$

$$\begin{aligned}\text{where } h(r) &= \frac{c_s}{\Omega} \\ &= 3.29 \times 10^{-2} \left(\frac{r}{1\text{au}}\right)^{\frac{5}{4}} \text{au},\end{aligned}\tag{13}$$

$$c_s(r) = \sqrt{\frac{k_B T(r)}{\mu m_p}},\tag{14}$$

$$\Omega_K(r) = \sqrt{\frac{GM_\odot}{r^3}},\tag{15}$$

$$v_K(r) = \sqrt{\frac{GM_\odot}{r}}.\tag{16}$$

species	$\sigma_{\text{inel}}$	$\sigma_{\text{el}}$
H <sub>2</sub>	$1.6 \times 10^{-16} \text{cm}^{-2}$	$6.6 \times 10^{-16} \text{cm}^{-2}$
He	$0.0 \text{cm}^{-2}$	$3.6 \times 10^{-16} \text{cm}^{-2}$
CO	$5.1 \times 10^{-18} \text{cm}^{-2}$	$1.1 \times 10^{-15} \text{cm}^{-2}$
O <sub>2</sub>	$1.8 \times 10^{-16} \text{cm}^{-2}$	$8.9 \times 10^{-16} \text{cm}^{-2}$

Table 1: Collisional cross sections of the molecules for 15eV electrons.

Here  $\mu m_p$  is the mean molecular mass of the gas. **Therefore the number density of H<sub>2</sub> is**

$$n_{\text{H}_2}(r, z) = 1.52 \times 10^{14} \exp\left(-\frac{z^2}{2h^2}\right) \frac{\Sigma(r)}{\Sigma(1\text{au})} \text{cm}^{-3}. \quad (17)$$

## 2.4. Breakdown Models on Protoplanetary Disks

Here we estimate the dielectric strength of the protoplanetary disk gas. **In our disk model the gas density at the equatorial plane,  $r = 1\text{au}$  is  $n_{0,\text{ppd}} = 1.52 \times 10^{14} \text{cm}^{-3}$ .** We assume that protoplanetary disk gas consists of H<sub>2</sub>, He, CO, O<sub>2</sub> and their volume fractions are 0.92,  $7.8 \times 10^{-2}$ ,  $2.3 \times 10^{-4}$ ,  $1.3 \times 10^{-4}$ , respectively (Lodders et al. 2009, chap. 3.4.6.) . We used cross sections data for 15eV electrons tabulated in (Itikawa. 2000; Martienssen 2003) (c.f. Table 1), since  $\Delta W_{\text{H}_2} = 15.43\text{eV}$  and 15eV is the closest table index that is found in the database.

Calculations similar to those in the previous section lead to the following values:

$$\begin{aligned}
E_{\text{c,T}} &= \frac{\Delta W}{e}(\sigma_{\text{inel}})n_n = 3.0 \times 10^{-1} \left( \frac{n_n}{n_{0,\text{ppd}}} \right) \text{V/cm}, \\
E_{\text{c,DP}} &= \frac{\Delta W}{0.43} \sqrt{\frac{m_e}{M}} \sigma_{\text{el}} n_n = 5.0 \times 10^{-2} \left( \frac{n_n}{n_{0,\text{ppd}}} \right) \text{V/cm}, \\
E_{\text{c,R}} &= \frac{e^3 a_{\text{min}} \bar{Z}}{8\pi\epsilon_0 m c^2} n_n = 1.4 \times 10^{-3} \left( \frac{n_n}{n_{0,\text{ppd}}} \right) \text{V/cm}.
\end{aligned} \tag{18}$$

### 3. OBSERVATION

#### 3.1. Calculation of the Terminal Velocity of the Ions

The goal of this section is to calculate the Doppler broadening of the molecular ion lines in the disk, which reflects the electric field strength in the protoplanetary disk. In order to establish the observation procedure, we calculate the collisional cross sections and the terminal velocities of the molecules. Then, we can estimate the optical depths and the spectral irradiances of the specific lines. We simulate the observational images using the calculated spectral irradiances. Finally, we establish a model discrimination procedure based on matched-filtering.

We choose three ion species:  $\text{HCO}^+$ ,  $\text{DCO}^+$  and  $\text{N}_2\text{H}^+$  lines, whose observations have been performed (Öberg et al. 2011, 2010). Such charged chemical species are accelerated upto their respective terminal velocity by the electric field of the LMG. Let  $\varepsilon_I$  be the kinetic energy of a particle of such an ion species  $I$ . We can calculate the value of  $\varepsilon_I$  at the equilibrium by solving

$$\kappa_{I,n} \varepsilon_I = e E_{\text{crit}} l_{\text{mfp},I}, \tag{19}$$

Here,  $\kappa_{I,n} = \frac{2m_I m_n}{(m_I + m_n)^2}$  is the fraction of ion energy loss per collision, and  $m_I$  and  $m_n$  are the masses of the ion and the neutral molecules, respectively (Golant et al. 1980).

As shown in equations (9) and (18), the dielectric strength  $E_{\text{crit}}$  is proportional to the gas number density  $n_n$ . Let  $A$  be the proportionality factor and  $E_{\text{crit}} = An_n$ . Now, the mean free path  $l_{\text{mfp},I} = 1/\sigma_I(\varepsilon_I)n_n$  is inversely proportional to the gas number density  $n_n$ . This means that the obtained kinetic energy  $\varepsilon_I$  is independent of the gas number density.

$$\begin{aligned}\varepsilon_I &= eE_{\text{crit}}l_{\text{mfp},I}(\kappa_{I,n})^{-1} \\ &= \frac{eA(m_I + m_n)^2}{2\sigma_I(\varepsilon_I)m_I m_n}\end{aligned}$$

The value of  $A$  only depends on the lightning model, so it is universally the same in a protoplanetary disk. **This feature is what we propose as a new signal of the lightning models in the disk. Recall that the proportionality factor  $A$  for the three lightning models are given as  $E_{\text{crit}} = An_n$  in Equations (18).** The predicted  $\varepsilon_I$  and the velocities of the ion species are shown in Table 2. In the Appendix we describe the detail of the cross section model we have used in order to estimate the above cross sections.

### 3.2. Estimation of the Observational Signals

The column density corresponding to optical depth  $\tau_{\nu 0} = 1$  is estimated as follows (see the appendix of Scoville et al. 1986):

$$N_{\tau_{\nu 0}=1} = \frac{3\epsilon_0 k_B T_{\text{ex}} \Delta v_{\text{gas}}}{2\pi^2 B \mu^2 \cos \theta} \frac{1}{(J+1)} \exp\left(\frac{hBJ(J+1)}{k_B T_{\text{ex}}}\right) \left(1 - \exp\left(-\frac{h\nu_0}{k_B T_{\text{ex}}}\right)\right), \quad (20)$$

where  $T_{\text{ex}}$  is the excitation temperature,  $\Delta v_{\text{gas}}$  is the Doppler broadening of the target molecule,  $B$  is the rotational constant of the molecule,  $\mu$  is its electric dipole matrix element,  $\theta$  is the angle between the disk axis and the line of sight,  $h\nu_0$  is the energy difference between the two levels and  $J$  is the rotational quantum number of the lower state.

Cross Section Model XL			
	HCO <sup>+</sup>	DCO <sup>+</sup>	N <sub>2</sub> H <sup>+</sup>
T	$8.6 \times 10^4$ cm/s	$8.6 \times 10^4$ cm/s	$8.6 \times 10^4$ cm/s
DP	$2.5 \times 10^4$ cm/s	$2.5 \times 10^4$ cm/s	$2.5 \times 10^4$ cm/s
R	$2.2 \times 10^3$ cm/s	$2.2 \times 10^3$ cm/s	$2.2 \times 10^3$ cm/s

Cross Section Model XM			
	HCO <sup>+</sup>	DCO <sup>+</sup>	N <sub>2</sub> H <sup>+</sup>
T	$4.2 \times 10^5$ cm/s	$4.2 \times 10^5$ cm/s	$4.2 \times 10^5$ cm/s
DP	$1.2 \times 10^5$ cm/s	$1.2 \times 10^5$ cm/s	$1.2 \times 10^5$ cm/s
R	$1.1 \times 10^4$ cm/s	$1.1 \times 10^4$ cm/s	$1.1 \times 10^4$ cm/s

Cross Section Model XS			
	HCO <sup>+</sup>	DCO <sup>+</sup>	N <sub>2</sub> H <sup>+</sup>
T	$2.0 \times 10^6$ cm/s	$2.0 \times 10^6$ cm/s	$2.0 \times 10^6$ cm/s
DP	$5.9 \times 10^5$ cm/s	$5.9 \times 10^5$ cm/s	$5.9 \times 10^5$ cm/s
R	$5.2 \times 10^4$ cm/s	$5.2 \times 10^4$ cm/s	$5.2 \times 10^4$ cm/s

Table 2: The terminal velocities of the molecular ions, for cross section models XL, XM and XS. The terminal velocities are the characteristic features we use for observational measurement of the dielectric strength.

The optical depth of the disk with column density  $N$  is

$$\tau_{\nu_0}(N) = N/N_{\tau_{\nu_0}=1}, \quad (21)$$

so that the intensity is

$$I(\nu_0) = B(\nu_0, T) (1 - \exp(-\tau_{\nu_0}(N))). \quad (22)$$

Here  $B(\nu_0, T)$  is the vacuum brightness of a black body at frequency  $\nu_0$  (see Lang (2006, chap. 2.7)).

The spectral irradiance of the disk  $E(\nu)$  as a function of  $\nu$  is

$$E(\nu) = \frac{1}{D^2} \int \int I(\nu_0, r) \exp\left(-\frac{mc^2 d(\nu; \nu_0, r)^2}{2k_B T \nu_0^2}\right) r dr d\varphi \cos \theta, \quad (23)$$

where  $d(\nu; \nu_0, r) = \nu - \nu_0 - \frac{v_K(r)}{c} \cos \varphi \sin \theta$ .

The integral is done in cylindrical coordinates  $(r, \phi)$ , and  $\theta$  is the inclination angle of the disk.

We consider  $\text{HCO}^+ 3 - 2$ ,  $\text{DCO}^+ 3 - 2$  and  $\text{N}_2\text{H}^+ 3 - 2$  lines. Their frequencies are 267.56GHz, 216.12GHz and 279.52GHz, respectively. At 100au of the model disk  $T = 27\text{K}$ .

For simplicity we assume that fractional abundances of the ion species are uniform within the disk. The population of the ionized species can be drastically increased or decreased as a result of lightning, but to estimate such population is beyond the scope of this paper. We adopt the XR+UV-new chemical process model of Walsh et al. (2012), and use the abundance values at  $r = 100\text{au}$ ,  $z = 3h$ , since the electric field is most likely to reach the critical amplitude at higher altitudes of the disk (Muranushi et al. 2012). Thus, we assume that the fractional abundances (relative to  $\text{H}_2$ ) of  $\text{N}_2\text{H}^+$  is  $5.3 \times 10^{-10}$ . We assume the fractional abundance of  $\text{HCO}^+$  and  $\text{DCO}^+$  to be  $9.0 \times 10^{-9}$  and  $3.0 \times 10^{-9}$ , respectively, based on paper by Mathews et al. (2013) that reports observation of enhancement in  $\text{DCO}$  abundance. Therefore, the column densities of  $\text{HCO}^+$ ,  $\text{DCO}^+$  and  $\text{N}_2\text{H}^+$  are  $1.8 \times 10^{15}\text{cm}^{-2}$ ,  $6.0 \times 10^{14}\text{cm}^{-2}$ , and  $1.1 \times 10^{14}\text{cm}^{-2}$ , respectively.

Assuming that there is no lightning and that the molecules are in their thermal velocities,  $N_{\tau_{\nu 0}=1}$  for the three lines are  $7.78 \times 10^9 \text{ cm}^{-2}$ ,  $6.74 \times 10^9 \text{ cm}^{-2}$  and



$1.39 \times 10^{10} \text{ cm}^{-2}$ , respectively. On the other hand,  $N_{\tau_{\nu 0}=1}$  for the three lines are  $6.15 \times 10^{11} \text{ cm}^{-2}$ ,  $5.42 \times 10^{11} \text{ cm}^{-2}$  and  $1.10 \times 10^{12} \text{ cm}^{-2}$ , respectively, if the molecules are accelerated by the lightning electric field.

We can see that the disk is optically thick for all of the lines at 100au. However, all the three lines become two degrees of magnitude more transparent under the effect of the critical electric field. This is a result of the molecular speed becoming faster. Consequently, observed line profiles are broadened. This Doppler broadening of the lines of the charged molecular species are the key observational features to observe the characteristic speed of the molecules, and therefore the electric field strength in the protoplanetary disk.

### 3.3. Calculations of the Line Profiles and Integral Maps by Radiative Transfer

We introduce seven disk models, as in Table 3. We calculate the line profiles for the three ion species with these seven disk models, in order to study the ability to distinguish the lightning model from the line observations (Figure 1). The line profiles are obtained by performing the spectral irradiance integral (equation (23)). We assume isotropic distribution for the ion velocities, assuming that the electric field is turbulent. We simulate the channel maps using the spectral line radiation transfer code LIME by Brinch & Hogerheijde (2010). In Figure 2, we present the simulated channel maps maps of the  $\text{HCO}^+$  line for N, T25, and T50 disk. We assumed that our model disk is located in the same way as TW Hya. That is, our model disk at the distance of 54 pc and the inclination angle of  $7^\circ$  (van Leeuwen 2007). Although we limit the disk parameters to this specific distance and inclination throughout this paper, our programs can be easily applied to other disk parameters.

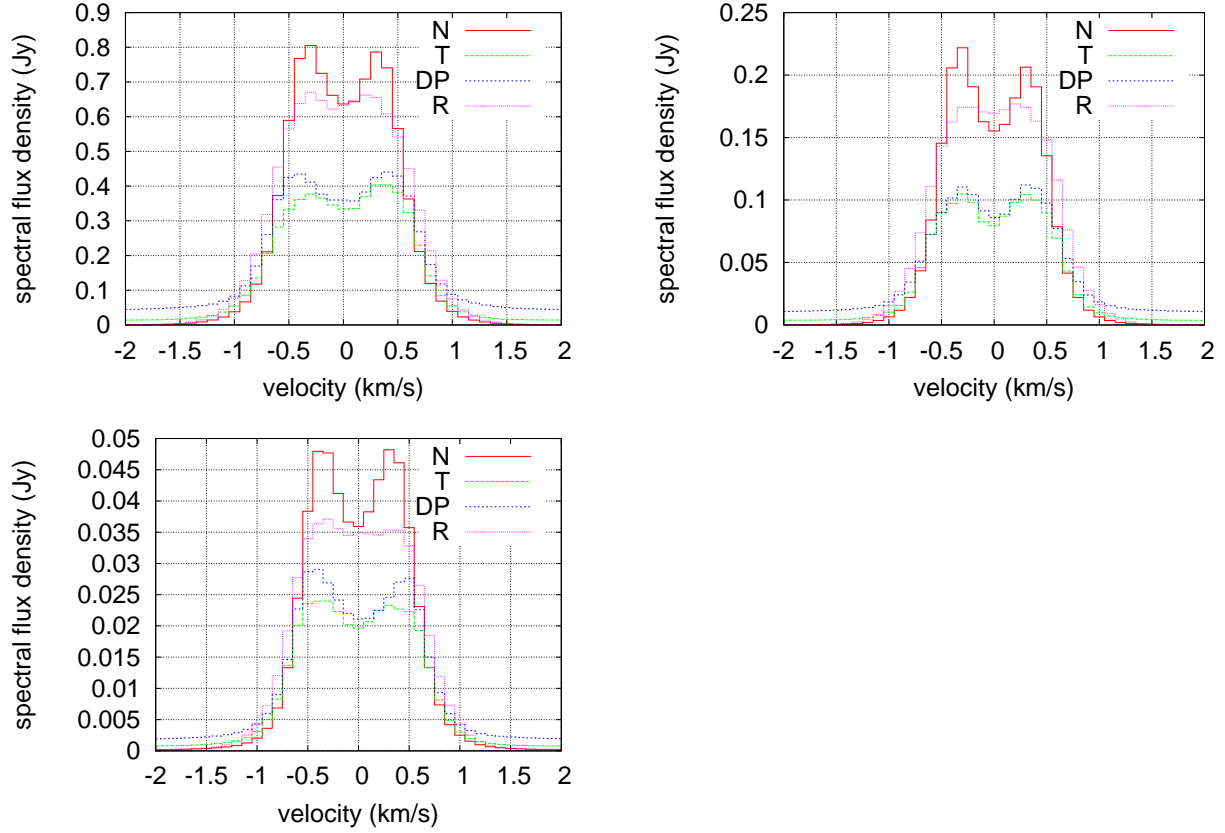


Fig. 1.— The line profiles for  $\text{HCO}^+$ ,  $\text{DCO}^+$  and  $\text{N}_2\text{H}^+$ , assuming that the lightning takes place at  $50\text{au} < r < 100\text{au}$  of the disk. The labels no, T, DP, and R for the curves corresponds to no lightning, Townsend breakdown model, Druyversteijn-Penning breakdown model and runaway breakdown model, respectively.

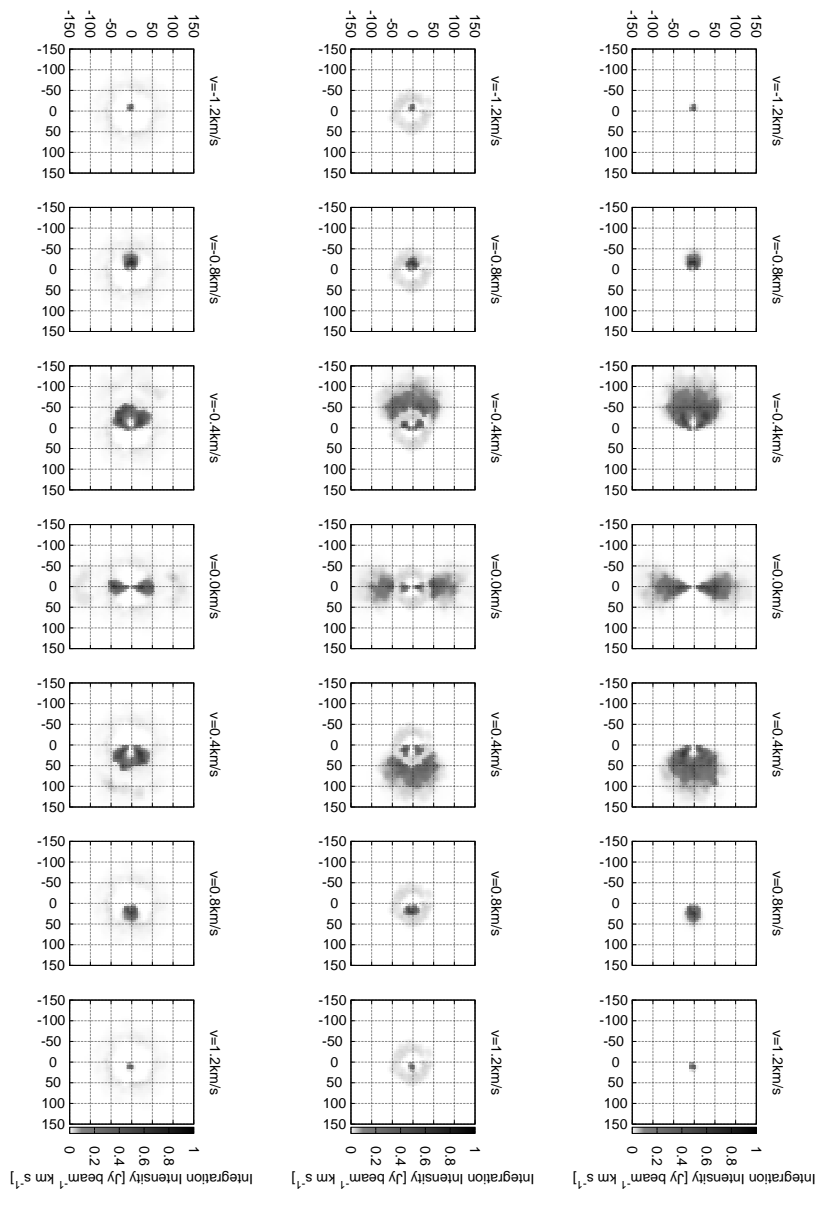


Fig. 2. — Simulated channel maps of  $\text{HCO}^+$  lines for disk models N (upper row), T25 (middle row), and T50 (lower row), respectively. Units are in  $\text{Jy beam}^{-1} \text{ km s}^{-1}$ . We assume the beam size of  $0''.65 \times 0''.44$ .

### 3.4. Matched Filtering

We apply the matched filtering method (North 1963), in order to distinguish lightning model by ALMA. Matched filtering is the optimal method for discriminating models under noisy observation has been well studied and have wide applications not only in radio astronomy (Ellingson & Hampson 2003) but also in extra solar planet astronomy (Jenkins et al. 1996; Doyle et al. 2000), gravitational wave astronomy (Owen & Sathyaprakash 1999; Vaishnav et al. 2007; Hotokezaka et al. 2013), and even in ocean tomography (Munk & Wunsch 1979). We follow the treatment by Creighton & Anderson (2011) .

Given that the noise levels for  $\text{HCO}^+$ ,  $\text{DCO}^+$  and  $\text{N}_2\text{H}^+$  are  $1.130 \times 10^{-2}$  Jy,  $1.330 \times 10^{-2}$  Jy, and  $1.800 \times 10^{-2}$  Jy, respectively, their noise spectrum power density  $S_h$  per square arcsecond are  $5.843 \times 10^{-5}$  Jy<sup>2</sup> km/s,  $8.094 \times 10^{-5}$  Jy<sup>2</sup> km/s, and  $1.483 \times 10^{-4}$  Jy<sup>2</sup> km/s, respectively.

The measure-of-sensitivity  $\sigma_{\text{mos}}$  of the matched-filter between two images  $h_1(x, y, v)$  and  $h_2(x, y, v)$  is:

$$\sigma_{\text{mos}} = 4 \int_{v_{\min}}^{v_{\max}} \int_{(x,y) \in \text{image}} \frac{|h_1(x, y, v) - h_2(x, y, v)|^2}{S_h} dx dy dv. \quad (24)$$

Here,  $x$  and  $y$  are image coordinates in arcseconds, and  $v$  is the velocity coordinate.

The measure of sensitivity among the models using different lines are summarized in Table 4. The measure-of-sensitivity for any two different models is larger than 100, and the largest measure-of-sensitivity is greater than 1000. Therefore the image like Figure 2 is not difficult to detect. However, no observation of protoplanetary disk has been reported. Therefore, we can reject such form of lightning models from observations. There are multiple alternative scenarios that observations suggest: (1) Protoplanetary disk lightning does not exist at all. (2) The probability of protoplanetary disk with lightning matrix gas

(LMG) is low, so that we have not yet observed one yet. (3) Protoplanetary disk LMG exists in forms of LMG clumps (protoplanetary “cumulonibus clouds”) much smaller than the size of the protoplanetary disks, (4) Planetary disk LMG is scattered in many smaller clumps in the protoplanetary disk with certain volume-filling factor, so that their total cross sections cover a fraction of the disk image. This case is reduced to case (3) by considering the total cross section of the clumps.

We can put the upper limit to the size of such LMG clumps by thresholding the measure-of-sensitivity. For example, if the radii of LMG clumps is smaller than the values in Table 6, they are not  $5.0 - \sigma$  detectable. The matched filter studies show that the Townsend breakdown model is the easiest model to detect, Druyversteijn-Penning model being next, runaway breakdown being most difficult. The tendency is explained as the wider the Doppler broadening is, more easier is the detection.

#### 4. CONCLUSIONS AND DISCUSSIONS.

Discharge phenomena take place in the regions with the critical electric field (LMG), and we have established observable features for detecting LMGs by the line observations of the accelerated molecular ions. Dielectric strength of the disk gas, being one of the crucial elementary processes, will open up the understanding of the MRI in protoplanetary disks. Understanding of the MRI in weakly-ionized accretion disks will contribute to the study of the dynamics of protoplanetary disks as well as circumplanetary disks (Keith & Wardle 2014).

We have presented three dielectric strength models for protoplanetary disks. They are Townsend breakdown model, Druyversteijn-Penning breakdown model, and runaway breakdown model, respectively. We have proposed a method for observational

distinguishment of the three models. The models are distinguishable with the sensitivity of advanced telescopes such as ALMA. It is now possible to reject some of the lightning models based on ground observations. The upper limits of the LMG clouds size are given from the observations.

Our lightning models treated here are quite simple. Further studies are targeting to apply this work to more realistic disk models as well as more detailed discharge models (Okuzumi & Inutsuka 2015).

### Acknowledgement

We thank Yasuo Fukui, Hitoshi Miura, Munetake Momose and Takayuki Muto for helpful discussions; Shinichi Enami for his advices on ice surface charge chemistry; Edward Kmett, Simon Peyton Jones and Richard Eisenberg for their comments on our Haskell programs; Tooru Eguchi for instruction of Japanese Virtual Observatory; Motomichi Tashiro for discussion on empirical formula of ion-molecule collision cross section. We thank Steven Rieder and Keigo Nitadori in helping us correct grammatical errors. We are grateful to Institute of Low Temperature Science, Hokkaido University for hosting the workshop “Recent Development in Studies of Protoplanetary Disks with ALMA” where the authors learned ALMA image analysis. This work is based on the landmark review of terrestrial lightning by Takahashi (2009). The parallel computation techniques used in this work are based on Marlow (2013). We used `units` library (Muranushi & Eisenberg 2014) to thoroughly check for the consistency of physical dimensions and units in this paper. This work is supported by Grants-in-Aid for Scientific Research (#23103005, #24103506, #25887023, #26400224) from MEXT. This research used computational resources of the K computer provided by the RIKEN Advanced Institute for Computational Science(AICS). We thank RIKEN AICS for the support in conducting this research. **We thank the referee for the patient and**

constructive interaction, with which we have made a substantial improvement to this paper.

## A. CROSS SECTION MODEL OF ION-NEUTRAL MOLECULAR COLLISION

We establish the model of ion-neutral collisional cross sections as functions of collision energy, in collaboration with Motomichi Tashiro.

In order to compute the equilibrium speed under electric field for ion species  $\text{HCO}^+$ ,  $\text{DCO}^+$  and  $\text{N}_2\text{H}^+$ , we need the knowledge of the energy-dependent cross section of the collisions between the  $\text{H}_2$  and the ion species. However, no experimental values for such collisions exist. In general, collisional cross section data for molecular ions and molecules are scarce, due to the difficulty of setting up such collision experiments. On the other hand, quantum-mechanical simulation of such collision event would require upto 1 month per single collision (Tashiro, private comm.) and it requires many collision simulations with different collision parameters to establish a cross section value for one collision energy. The computational cost prohibits the simulational estimation of the collisional cross section.

Therefore, we construct and use a simple empirical model of molecular ions and molecules collisional cross section, following Tashiro’s advice.

There are collision cross section data (Phelps 1990, 1991). for the following six pairs of molecular ions and molecules:  $\text{H}^+ - \text{H}_2$ ,  $\text{H}_2^+ - \text{H}_2$ ,  $\text{H}_3^+ - \text{H}_2$ ,  $\text{N}^+ - \text{N}_2$ ,  $\text{N}_2^+ - \text{N}_2$ , and  $\text{Ar}^+ - \text{Ar}$ . We use the following model of total collisional cross section  $\sigma_{I^+,I}(\varepsilon)$  between molecular ion species  $I^+$  and ion species  $I$ :

$$\sigma_{I^+,I}(\varepsilon) = A(\varepsilon)\mu(I^+, I)^{p(\varepsilon)}, \quad (\text{A1})$$

where  $\varepsilon$  is the collision energy,  $\mu(I^+, I)$  is the residual mass of species  $I^+$  and  $I$ .  $A(\varepsilon)$  and

$p(\varepsilon)$  are model parameters **universal across all species**.

We perform the fitting of the model so that the following cost function  $C$

$$C = \sum_{\varepsilon, I^+, I} (\sigma_{I^+, I}(\varepsilon) - \sigma_{I^+, I, \text{exp}}[\varepsilon])^2 \quad (\text{A2})$$

is minimized. Here,  $\sigma_{I^+, I, \text{exp}}[\varepsilon]$  are experimentally known cross section values for some fixed values of  $\varepsilon$  found in Phelps (1990, 1991). The experimental data and the best-fit models are presented in Figure 3. Our cross section model predicts almost identical cross sections for the three collision pairs  $\text{HCO}^+ - \text{H}_2$ ,  $\text{DCO}^+ - \text{H}_2$ , and  $\text{N}_2\text{H}^+ - \text{H}_2$ . This is because our model depends only on the residual mass of species  $\mu(I^+, I)$ , and all the three pairs  $\text{HCO}^+ - \text{H}_2$ ,  $\text{DCO}^+ - \text{H}_2$ , and  $\text{N}_2\text{H}^+ - \text{H}_2$  have similar residual masses.

Available experimental data on ion-neutral collisional cross section are scarce, and do not justify models more complex than equation (A1). Instead of making better-fitting models, we study how the uncertainty in the model affects our results. In addition to the model equation (A1) with the fitted parameters (Figure 3), we study two alternative models, where

$$\sigma_{I^+, I}^{\text{L}}(\varepsilon) = 10\sigma_{I^+, I}(\varepsilon), \quad (\text{A3})$$

$$\sigma_{I^+, I}^{\text{S}}(\varepsilon) = \frac{1}{10}\sigma_{I^+, I}(\varepsilon), \quad (\text{A4})$$

for  $I^+ - I = \text{HCO}^+ - \text{H}_2$ ,  $\text{DCO}^+ - \text{H}_2$ , and  $\text{N}_2\text{H}^+ - \text{H}_2$ . The cross section models of equations (A1), (A3), and (A4), are labeled XM, XL, and XS, respectively.



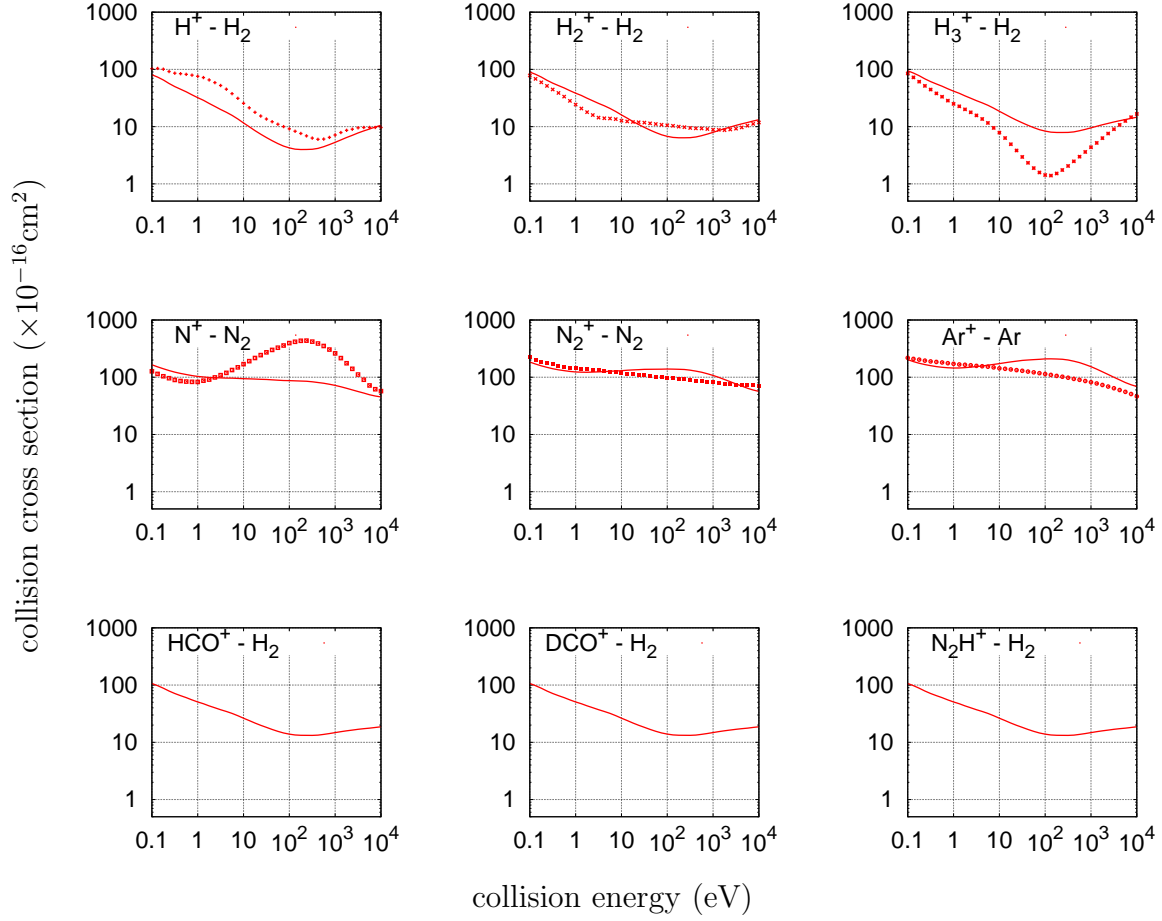


Fig. 3.— Cross section models. Experimental data are points, curves show the model XM.

disk model name	discharge	LMG region
N	no discharge	
T25	Townsend discharge	$25\text{au} < r < 50\text{au}$
T50	Townsend discharge	$50\text{au} < r < 100\text{au}$
DP25	Druyversteyn-Penning discharge	$25\text{au} < r < 50\text{au}$
DP50	Druyversteyn-Penning discharge	$50\text{au} < r < 100\text{au}$
R25	runaway discharge	$25\text{au} < r < 50\text{au}$
R50	runaway discharge	$50\text{au} < r < 100\text{au}$

Table 3: Our seven disk models, their respective discharge models and LMG distribution models.

HCO <sup>+</sup>	T25	DP25	R25
N	3729.7	3021.6	1277.1
T25		1508.4	3294.1
DP25			2608.7

HCO <sup>+</sup>	T50	DP50	R50
N	2488.4	2199.2	1277.4
T50		1418.7	2316.5
DP50			2125.5

DCO <sup>+</sup>	T25	DP25	R25
N	122.3	104.9	46.3
T25		44.7	115.3
DP25			99.3

DCO <sup>+</sup>	T50	DP50	R50
N	111.3	100.9	45.8
T50		42.8	95.3
DP50			81.6

N <sub>2</sub> H <sup>+</sup>	T25	DP25	R25
N	5.8	5.2	2.3
T25		2.0	5.8
DP25			5.1

N <sub>2</sub> H <sup>+</sup>	T50	DP50	R50
N	4.0	3.5	2.4
T50		2.3	3.8
DP50			3.4

3 species	T25	DP25	R25
N	3857.9	3131.7	1325.6
T25		1555.2	3415.1
DP25			2713.0

3 species	T50	DP50	R50
N	2603.7	2303.7	1325.6
T50		1463.9	2415.5
DP50			2210.4

Table 4: The measure of sensitivity values among N, T25, DP25 and R25 models, and among N, T50, DP50 and R50 models, using either one of, or all the three of, our lines HCO<sup>+</sup> 3 – 2 , DCO<sup>+</sup> 3 – 2 and N<sub>2</sub>H<sup>+</sup> 3 – 2.

XL

3 species	T25	DP25	R25	3 species	T50	DP50	R50
N	2872.2	1547.5	1193.0	N	2365.7	1539.3	1326.4
T25		1988.4	2813.6	T50		1539.7	2408.2
DP25			1543.8	DP50			1635.3

XM

3 species	T25	DP25	R25	3 species	T50	DP50	R50
N	3857.9	3131.7	1325.6	N	2603.7	2303.7	1325.6
T25		1555.2	3415.1	T50		1463.9	2415.5
DP25			2713.0	DP50			2210.4

XS

3 species	T25	DP25	R25	3 species	T50	DP50	R50
N	3483.7	3484.1	2101.3	N	2648.4	2623.6	2067.3
T25		1294.1	2315.4	T50		1170.2	1683.7
DP25			2217.8	DP50			1603.3

Table 5: The dependence of the measure of sensitivity on the cross section models. The measure of sensitivity was estimated among N, T25, DP25 and R25 models, and among N, T50, DP50 and R50 models, using all the three of, our lines  $\text{HCO}^+ 3 - 2$ ,  $\text{DCO}^+ 3 - 2$  and  $\text{N}_2\text{H}^+ 3 - 2$ .

XL

3 species	T25	DP25	R25	3 species	T50	DP50	R50
N	1.8 au	2.5 au	2.8 au	N	4.0 au	4.9 au	5.3 au
T25		2.2 au	1.8 au	T50		4.9 au	3.9 au
DP25			2.5 au	DP50			4.8 au

XM

3 species	T25	DP25	R25	3 species	T50	DP50	R50
N	1.6 au	1.7 au	2.7 au	N	3.8 au	4.0 au	5.3 au
T25		2.5 au	1.7 au	T50		5.1 au	3.9 au
DP25			1.9 au	DP50			4.1 au

XS

3 species	T25	DP25	R25	3 species	T50	DP50	R50
N	1.6 au	1.6 au	2.1 au	N	3.8 au	3.8 au	4.3 au
T25		2.7 au	2.0 au	T50		5.7 au	4.7 au
DP25			2.1 au	DP50			4.8 au

Table 6: The upper limits to the sizes of the LMG clumps that exist on  $25\text{au} < r < 50\text{au}$  and  $50\text{au} < r < 100\text{au}$  orbit, respectively.

## REFERENCES

- Akiyama, E., Momose, M., Kitamura, Y., Tsukagoshi, T., Shimada, S., Koyamatsu, S., & Hayashi, M. 2013, Publications of the Astronomical Society of Japan, 65, 123123
- Andrews, S. M., Wilner, D. J., Hughes, A. M., Qi, C., & Dullemond, C. P. 2009, ApJ, 700, 1502
- . 2010, ApJ, 723, 1241
- Berger, M., Coursey, J., Zucker, M., & Chang, J. 2009, Stopping-Power and Range Tables for Electrons, Protons, and Helium Ions (NIST, Physical Measurement Laboratory)
- Bethe, H. 1930, Annalen der Physik, 397, 325
- . 1932, Zeitschrift fr Physik, 76, 293
- Bloch, F. 1933, Zeitschrift fr Physik, 81, 363
- Brinch, C., & Hogerheijde, M. R. 2010, Astronomy and Astrophysics, 523, A25
- Calvet, N., D’Alessio, P., Hartmann, L., Wilner, D., Walsh, A., & Sitko, M. 2002, ApJ, 568, 1008
- Chantry, P. J. 1981, Journal of Applied Physics, 52, 2731
- Creighton, J. D. E., & Anderson, W. G. 2011, Gravitational wave physics and astronomy an introduction to theory, experiment and data analysis (Weinheim: Wiley-VCH-Verl.)
- Desch, S., & Cuzzi, J. 2000, Icarus, 143, 87
- Desch, S. J., & Cuzzi, J. N. 2000, Icarus, 143, 87

- Doyle, L. R., Deeg, H. J., Kozhevnikov, V. P., Oetiker, B., Martín, E. L., Blue, J. E., Rottler, L., Stone, R. P. S., Ninkov, Z., Jenkins, J. M., Schneider, J., Dunham, E. W., Doyle, M. F., & Paleologou, E. 2000, *ApJ*, 535, 338
- Druyvesteyn, M. J., & Penning, F. M. 1940, *Reviews of Modern Physics*, 12, 87
- Dye, J. E., Jones, J. J., Winn, W. P., Cerni, T. A., Gardiner, B., Lamb, D., Pitter, R. L., Hallett, J., & Saunders, C. P. R. 1986, *Journal of Geophysical Research*, 91, 1231
- Ellingson, S. W., & Hampson, G. A. 2003, *ApJS*, 147, 167
- French, J. R., Helsdon, J. H., Detwiler, A. G., & Smith, P. L. 1996, *Journal of Geophysical Research*, 101, 18961
- Gibbard, S., E.H., L., & Morfill, G. E. 1997, *Icarus*, 130, 517533
- Golant, V. E., Zhilinskii, A. P., & Sakharov, I. E. 1980, *Fundamentals of plasma physics* (Wiley New York)
- Gurevich, A., Milikh, G., & Roussel-Dupre, R. 1992, *Physics Letters A*, 165, 463
- Gurevich, A. V., & Zybin, K. P. 2001, *Physics-Uspekhi*, 44, 1119
- Hayashi, C. 1981, *Progress of Theoretical Physics Supplement*, 70, 35
- Hotokezaka, K., Kiuchi, K., Kyutoku, K., Muranushi, T., Sekiguchi, Y.-i., Shibata, M., & Taniguchi, K. 2013, *Phys. Rev. D*, 88, 044026
- Hubbard, A., McNally, C. P., & Mac Low, M.-M. 2012, *ApJ*, 761, 58
- Inutsuka, S., & Sano, T. 2005, *The Astrophysical Journal*, 628, L155
- Itikawa., Y. 2000, *Interactions of photons and electrons with atoms* (Berlin [u.a.]: Springer)
- . 2001, *Collisions of electrons with atomic ions* (Berlin [u.a.]: Springer)

- Jenkins, J. M., Doyle, L. R., & Cullers, D. K. 1996, *Icarus*, 119, 244
- Keith, S. L., & Wardle, M. 2014, *MNRAS*, 440, 89
- Kitamura, Y., Momose, M., Yokogawa, S., Kawabe, R., Tamura, M., & Ida, S. 2002, *ApJ*, 581, 357
- Lang, K. R. 2006, *Astrophysical formulae* (Berlin: Springer)
- Lodders, K., Palme, H., & Gail, H.-P. 2009, *Landolt Börnstein*, 44
- Longair, M. S. 2010, *High energy astrophysics* (Cambridge: Cambridge University Press)
- Mansell, E. R., MacGorman, D. R., Ziegler, C. L., & Straka, J. M. 2002, *Journal of Geophysical Research (Atmospheres)*, 107, 4075
- Marlow, S. 2013, *Parallel and Concurrent Programming in Haskell*. (Oreilly & Associates Inc)
- Martienssen, W. 2003, *Interactions of photons and electrons with molecules* (Berlin [u.a.]: Springer)
- Mathews, G. S., Klaassen, P. D., Juhász, A., Harsono, D., Chapillon, E., van Dishoeck, E. F., Espada, D., de Gregorio-Monsalvo, I., Hales, A., Hogerheijde, M. R., Mottram, J. C., Rawlings, M. G., Takahashi, S., & Testi, L. 2013, *A&A*, 557, A132
- McNally, C. P., Hubbard, A., Mac Low, M.-M., Ebel, D. S., & D’Alessio, P. 2013, *ApJ*, 767, L2
- Menu, J., van Boekel, R., Henning, T., Chandler, C. J., Linz, H., Benisty, M., Lacour, S., Min, M., Waelkens, C., Andrews, S. M., Calvet, N., Carpenter, J. M., Corder, S. A., Deller, A. T., Greaves, J. S., Harris, R. J., Isella, A., Kwon, W., Lazio, J., Le



- Bouquin, J.-B., Ménard, F., Mundy, L. G., Pérez, L. M., Ricci, L., Sargent, A. I., Storm, S., Testi, L., & Wilner, D. J. 2014, *A&A*, 564, A93
- Munk, W., & Wunsch, C. 1979, *Deep Sea Research A*, 26, 123
- Muranushi, T. 2010, *MNRAS*, 401, 2641
- Muranushi, T., & Eisenberg, R. A. 2014, *Proceedings of the 2014 ACM SIGPLAN symposium on Haskell - Haskell 14*, 31
- Muranushi, T., Okuzumi, S., & Inutsuka, S.-i. 2012, *ApJ*, 760, 56
- Nasser, E. 1968, *Journal of Applied Physics*, 39, 3707
- North, D. 1963, *Proceedings of the IEEE*, 51, 10161027
- Öberg, K. I., Qi, C., Fogel, J. K. J., Bergin, E. A., Andrews, S. M., Espaillat, C., van Kempen, T. A., Wilner, D. J., & Pascucci, I. 2010, *ApJ*, 720, 480
- Öberg, K. I., Qi, C., Fogel, J. K. J., Bergin, E. A., Andrews, S. M., Espaillat, C., Wilner, D. J., Pascucci, I., & Kastner, J. H. 2011, *ApJ*, 734, 98
- Okuzumi, S., & Inutsuka, S.-i. 2015, *ApJ*, 800, 47
- Owen, B. J., & Sathyaprakash, B. S. 1999, *Phys. Rev. D*, 60, 022002
- Phelps, A. V. 1990, *Journal of Physical and Chemical Reference Data*, 19, 653
- . 1991, *Journal of Physical and Chemical Reference Data*, 20, 557
- Phelps, C. T. 1971, *Journal of Geophysical Research*, 76, 57995806
- Phelps, C. T., & Griffiths, R. F. 1976, *Journal of Applied Physics*, 47, 2929
- Pilipp, W., Hartquist, T. W., & Morfill, G. E. 1992, *ApJ*, 387, 364

- Pilipp, W., Hartquist, T. W., Morfill, G. E., & Levy, E. H. 1998, *A&A*, 331, 121
- Raizer, Y. P. 1997, *Gas discharge physics* (Berlin: Springer)
- Rigden, J. S. 1996, [A - D]. (New York: Macmillan Reference USA)
- Scoville, N. Z., Sargent, A. I., Sanders, D. B., Claussen, M. J., Masson, C. R., Lo, K. Y., & Phillips, T. G. 1986, *ApJ*, 303, 416
- Takahashi, T. 1983, *Journal of the Meteorological Society of Japan*. Ser. II, 61, 656
- . 2009, *Kaminari no Kagaku* (Tokyo Daigaku Shuppankai)
- Takahashi, T., Tajiri, T., & Sonoi, Y. 1999, *Journal of Atmospheric Sciences*, 56, 1561
- Vaishnav, B., Hinder, I., Herrmann, F., & Shoemaker, D. 2007, *Phys. Rev. D*, 76, 084020
- van Leeuwen, F., ed. 2007, *Astrophysics and Space Science Library*, Vol. 350, *Hipparcos, the New Reduction of the Raw Data*
- Walsh, C., Nomura, H., Millar, T. J., & Aikawa, Y. 2012, *The Astrophysical Journal*, 747, 114
- Wasilewski, P., & Dickinson, T. 2000, *Meteoritics and Planetary Science*, 35, 537
- Williams, J. P., & Cieza, L. A. 2011, *Annual Review of Astronomy and Astrophysics*, 49, 67